On the Stability and Robustness of Model Predictive Direct Current Control

Tobias Geyer, Ricardo P. Aguilera and Daniel E. Quevedo

***Abstract*—Model predictive direct current control (MPDCC) has emerged as a promising control scheme for high-power power electronic applications, achieving very low current distortion levels and fast dynamic responses. This is achieved by addressing the current control and the modulation problems in one computational stage. For MPDCC the issue of closed-loop stability has not yet been investigated. In this paper, it will be shown that the MPDCC algorithm guarantees stability, i.e. the load currents are moved into given bounds and kept inside of these bounds. It will also be shown that—by slightly modifying the MPDCC algorithm—robustness to parameter uncertainties can be established.**

I. Introduction

Model predictive control (MPC) for power electronics has received a lot of attention during the past few years—both in academia as well as in industry. The availability of ubiquitous and cheap computational hardware has facilitated this rise. For three-phase AC systems, broadly speaking, MPC without a subsequent modulator can be classified into two main groups, namely MPC with reference tracking of the controlled variables, and MPC with (upper and lower) bounds imposed on the controlled variables.

The main advantage of the first group, MPC with reference tracking, is its simplicity and versatility [7]. It appears to be particularly well suited for low voltage applications where the pulse number (switching frequency divided by the fundamental frequency) tends to be high, typically exceeding 50.

In contrast to that, the second group, MPC with bounds on the controlled variables, excels for systems with very low pulse numbers in the single digit range. Its advantages are very low current distortion levels for a given pulse number, or, conversely, a very low switching effort (i.e. switching frequency or losses) for a given current distortion level. However, the computations required to solve the underlying optimization problem are often fairly demanding.

The model predictive direct control family (MPDxC) with $x \in \{T, C, P, B\}$, representing the torque, current, power and balancing, respectively, has been established over the past decade. More specifically, model predictive direct torque (MPDTC) was proposed in 2005 [8], [16] as a successor of DTC [26] and generalized in 2009 to arbitrary switching horizons [9]. At steady-state operating conditions, MPDTC provides switching losses and current distortions similar to the ones typically achieved by optimized pulse patterns [6], while during transients, its dynamic response is as fast as the one of DTC [10]. Model predictive direct current control (MPDCC) is a derivative of MPDTC [13], while model predictive direct power control (MPDPC) is the adaptation of MPDTC to grid-connected converters [17]. Model predictive direct balancing control (MPDBC) is the most recent member of the family, being used to control the internal voltages of multi-level converters [19].

Numerous studies have confirmed that MPC has the potential to provide significant performance gains, when compared to more traditional control methods, in particular when converters are operated outside of their basic regimens; see e.g., [3], [21], [22].

Despite the good performance that MPC formulations for power converters in principle offer, there remain several open problems, being one of the most important, the stability issue.

Recently, in [1], a stability analysis of power converters governed by MPC has been presented. The distinguishing aspect of this analysis is that power converters are modeled as linear systems, where the input vector, i.e. the switching positions or converter voltage levels, is restricted to belong to a finite set of possible control actions. For this setup, Lyapunov stability in a neighborhood of the desired reference can be established; see [2], [23] for a in depth presentation.

Another approach to model power converters is to interpret them as hybrid or switched (non)linear systems [25]. Power converters can be described by a set of discrete operation modes with associated continuous dynamics (involving voltages, currents, etc.). Switching triggers events that lead to jumps between the modes. Based on this approach, in [15], a so-called $\nu-$resolution model was introduced to obtain a piecewise-affine form of the system, based on which an explicit MPC solution can be obtained in an offline procedure [4]. The disadvantage of this approach stems from the fact that the control law's complexity (number of regions) grows exponentially with the length of the prediction horizon. For more details about the stability of hybrid systems governed by MPC the reader is referred to [20].

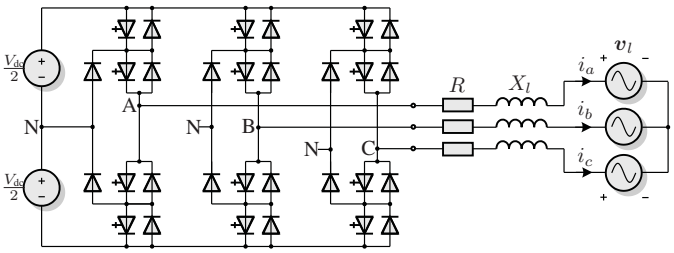

Fig. 1: Three-level neutral point clamped voltage source converter with a fixed neutral point potential connected to an active resistive-inductive load

T. Geyer is with ABB Corporate Research, 5405 Baden-Dättwil, Switzerland (e-mail: t.geyer@ieee.org). R. P. Aguilera and D. Quevedo are with the School of Electrical Engineering and Computer Science, The University of Newcastle, Australia (e-mails: aguilera.ricardo@gmail.com, dquevedo@ieee.org)

978-1-4673-4568-2/13/$31.00 ©2012 IEEE

So far, one important aspect has not yet been considered for the MPDxC family—closed-loop stability. For a key representative of this family, MPDCC, first results on closed-loop stability and robust stability will be presented in this contribution. The former can be directly established by the way the control algorithm has been designed. The reasoning is thus straightforward. For the latter—robust stability—a small modification in the algorithm is proposed that ensures robustness to bounded additive parameter uncertainties.

II. Case Study

Throughout this paper, we will use normalized quantities. Extending this to the time scale t, one time unit corresponds to $1/\omega_b$ seconds, where ω_b is the base angular velocity. Additionally, we will use $\xi(t)$, $t \in \mathbb{R}$, to denote continuous-time variables, and $\xi(k)$, $k \in \mathbb{N}$, to denote discrete-time variables with the sampling interval T_s.

A. The dq Reference Frame

All variables $\boldsymbol{\xi}_{abc} = [\xi_a \ \xi_b \ \xi_c]^T$ in the three-phase system (abc) are transformed to $\boldsymbol{\xi}_{dq} = [\xi_d \ \xi_q]^T$ in the orthogonal and rotating dq reference frame through $\boldsymbol{\xi}_{dq} = \boldsymbol{P}(\varphi)\,\boldsymbol{\xi}_{abc}$, where φ denotes the angle between the a-axis of the three-phase system and the d-axis of the reference frame. The reference frame rotates with the angular speed $\omega_{\text{fr}} = \mathrm{d}\varphi/\mathrm{d}t$. The transformation matrix is given by

$$\boldsymbol{P}(\varphi) = \frac{2}{3}\begin{bmatrix} \cos(\varphi) & \cos(\varphi - \frac{2\pi}{3}) & \cos(\varphi + \frac{2\pi}{3}) \\ -\sin(\varphi) & -\sin(\varphi - \frac{2\pi}{3}) & -\sin(\varphi + \frac{2\pi}{3}) \end{bmatrix}. \tag{1}$$

The stationary (i.e. non-rotating) $\alpha\beta$ reference frame is obtained by setting both φ and ω_{fr} to zero. The d- and q-axes are then referred to as α- and β-axes, respectively. The transformation from the abc to the $\alpha\beta$ reference frame is defined through $\boldsymbol{\xi}_{\alpha\beta} = \boldsymbol{P}(0)\,\boldsymbol{\xi}_{abc}$.

B. NPC Converter

As an example for a medium-voltage three-phase system, consider a three-level neutral point clamped (NPC) voltage source converter with an active resistive-inductive (RL) load, as shown in Fig. 1. The converter is fed by two constant dc-link voltage sources. The total dc-link voltage is V_{dc}.

Let the integer variables u_a, u_b, $u_c \in \{-1, 0, 1\}$ denote the switch positions in each phase leg, where the values $-1, 0, 1$ correspond to the phase voltages $-\frac{V_{\text{dc}}}{2}, 0, \frac{V_{\text{dc}}}{2}$, respectively. The single-phase switch positions can be aggregated to the three-phase switch position $\boldsymbol{u} = \boldsymbol{u}_{abc} = [u_a \ u_b \ u_c]^T$ with $\boldsymbol{u} \in \boldsymbol{\mathcal{U}} = \{-1, 0, 1\}^3$. The actual voltage at the converter terminals, commonly referred to as voltage vector, is given by

$$\boldsymbol{v}_{dq} = \frac{1}{2} V_{\text{dc}}\,\boldsymbol{P}(\varphi)\,\boldsymbol{u}_{abc}\,, \tag{2}$$

with $\boldsymbol{v}_{dq} \in \boldsymbol{\mathcal{V}}(\varphi)$, where the set $\boldsymbol{\mathcal{V}}(\varphi)$ is the image of $\boldsymbol{\mathcal{U}}$ when using the linear transformation (2).

C. Three-Phase Load

Consider a generic and symmetric three-phase load, as shown in Fig. 1. Each phase comprises the load resistor R, the inductor X_l and the voltage source $\boldsymbol{v}_l$. The latter vary sinusoidally over time with the frequency ω_e. The star point of the load is not connected.

This setup may, for example, represent an active front end connected to the grid, or the machine-side converter of an electrical drive with an AC machine. In the remainder of the paper we will consider the former setup[1].

Using vector notation, the load can be easily modeled in the dq reference frame

$$\frac{\mathrm{d}\boldsymbol{i}_{dq}}{\mathrm{d}t} = \frac{1}{X_l}(\boldsymbol{v}_{dq} - \boldsymbol{v}_{l,dq}) - \frac{R}{X_l}\boldsymbol{i}_{dq} - \omega_{\text{fr}}\begin{bmatrix} 0 & -1 \\ 1 & 0 \end{bmatrix}\boldsymbol{i}_{dq}\,, \tag{3}$$

where we set $\omega_{\text{fr}} = \omega_{\text{e}}$. As a result, the load voltage $\boldsymbol{v}_{l,dq}$ is time-invariant in this reference frame. Note that, according to (2), $\boldsymbol{v}_{dq}$ denotes the voltage at the converter terminals.

Correspondingly, an equivalent model of the load in $\alpha\beta$ coordinates is

$$\frac{\mathrm{d}\boldsymbol{i}_{\alpha\beta}}{\mathrm{d}t} = \frac{1}{X_l}(\boldsymbol{v}_{\alpha\beta} - \boldsymbol{v}_{l,\alpha\beta}) - \frac{R}{X_l}\boldsymbol{i}_{\alpha\beta}\,, \tag{4}$$

where the evolution of the load voltage can be described by

$$\frac{\mathrm{d}\boldsymbol{v}_{l,\alpha\beta}}{\mathrm{d}t} = \omega_e \boldsymbol{\Upsilon}\,\boldsymbol{v}_{l,\alpha\beta}\,, \quad \boldsymbol{\Upsilon} = \begin{bmatrix} 0 & -1 \\ 1 & 0 \end{bmatrix} \tag{5}$$

and an appropriate initial condition.

III. Control Problem Formulation

A. Control Problem

The current control problem at hand is to keep the three phase currents of the load, i_a, i_b and i_c, within upper and lower bounds around their respective reference values $i_{\text{ref},a}$, $i_{\text{ref},b}$ and $i_{\text{ref},c}$. Using symmetric bounds and letting δ_i denote the difference between the upper (lower) bound and a reference, the current constraints are given by

$$|i_{\text{ref},a} - i_a| \leq \delta_i\,, \quad |i_{\text{ref},b} - i_b| \leq \delta_i\,, \quad |i_{\text{ref},c} - i_c| \leq \delta_i\,. \tag{6}$$

To simplify the exposition in this paper, the hexagon-shaped set of bounds (6) is approximated by a circular bound with radius δ_i, centered at the three-phase reference current $\boldsymbol{i}_{\text{ref}} = [i_{\text{ref},a} \ i_{\text{ref},b} \ i_{\text{ref},c}]^T$. We thus impose

$$\boldsymbol{i} \in \boldsymbol{\mathcal{X}}_i\,, \quad \boldsymbol{\mathcal{X}}_i = \{\boldsymbol{i} \in \mathbb{R}^2 : ||\boldsymbol{i}_{\text{ref}} - \boldsymbol{i}||_2 \leq \delta_i\} \tag{7}$$

During step changes or transients, when bound violations might occur, the current is to be promptly moved back into its circular bound. As a metric for the degree of the violation serves the Euclidean distance between $\boldsymbol{i}$ and the closest point on the circle.

$$\boldsymbol{\epsilon}_i = ||\boldsymbol{i}_{\text{ref}} - \boldsymbol{i}||_2 - \delta_i\,, \quad \text{for } \boldsymbol{i} \notin \boldsymbol{\mathcal{X}}_i\,. \tag{8}$$

[1]The figures in this paper were created using the following set of per unit parameters: $V_{\text{dc}} = 1.93$, $R = 0.01$, $X_l = 0.2$, $v_l = 1$, $\omega_e = 1$, $\omega_{\text{fr}} = 1$, $i_{\text{ref}} = 0.6$ and $\delta_i = 0.15$. The sampling interval is $T_s = 25\,\mu$s.

At steady state operating conditions, the total harmonic distortion (THD) of the current is to be kept small. During transients, a high dynamic performance is to be ensured, i.e. a short current settling time in the range of a few ms. Moreover, with regard to the converter, the switching losses in the semiconductors are to be minimized. An indirect way of achieving this is to reduce the device switching frequency.

B. Set of Voltage Vectors

The set of discrete voltage vectors that can be synthesized by the NPC converter are contained in a circular set according to

$$\boldsymbol{v} \in \boldsymbol{\mathcal{X}}_{\mathrm{dc}}, \quad \boldsymbol{\mathcal{X}}_{\mathrm{dc}} = \{\boldsymbol{v} \in \mathbb{R}^2 : ||\boldsymbol{v}||_2 \leq \delta_{\mathrm{dc}}\}\,. \tag{9}$$

From (1) and (2) the radius of the enclosing circle can be calculated as $\delta_{\mathrm{dc}} = 2/3 V_{\mathrm{dc}}$. The envelope of $\boldsymbol{\mathcal{X}}_{\mathrm{dc}}$ is shown in Fig. 2 as a dashed (black) circle.

C. Control Principle

The control principle of direct current control is best explained in the rotating dq reference frame, as shown in Fig. 2. The controller operates in the discrete-time domain with the switch positions held constant during the sampling interval T_s. Assuming a power factor of one, the load voltage $\boldsymbol{v}_l$ and the current reference $\boldsymbol{i}_{\mathrm{ref}}$ are co-linear and are chosen to be aligned with the d-axis.

The forward Euler approximation of (3) yields at time-step k the discrete time-domain representation

$$\boldsymbol{i}(k+1) = \boldsymbol{i}(k) + \frac{T_s}{X_l}(\boldsymbol{v}(k) - \boldsymbol{v}_{ss}(k))\,, \tag{10}$$

where we have omitted the dq indices to simplify the notation and introduced

$$\boldsymbol{v}_{ss}(k) = \boldsymbol{v}_l(k) + \big(R + \omega_{\mathrm{fr}} \boldsymbol{\Upsilon} X_l\big)\boldsymbol{i}(k)\,. \tag{11}$$

Assume, as shown in Fig. 2, $\boldsymbol{i}(k)$ to have hit the circular bound. A voltage vector $\boldsymbol{v}(k)$ needs to be chosen that keeps the current within its bound. Note that the voltage difference $\boldsymbol{v}(k) - \boldsymbol{v}_{ss}(k)$ drives the required change in the current.

Using (10) the circular current bound can be translated into a circular voltage bound, partly depicted as a large dashed (blue) circle in Fig. 2. Correspondingly, the current set region $\boldsymbol{\mathcal{X}}_i$ can be translated into a voltage set region $\boldsymbol{\mathcal{X}}_v$. The selection of any voltage vector that is contained in this circle, $\boldsymbol{v}(k) \in \boldsymbol{\mathcal{X}}_{\boldsymbol{v}}$, ensures $\boldsymbol{i}(k+1) \in \boldsymbol{\mathcal{X}}_{\boldsymbol{i}}$, namely the current will be kept within its bound. The set of available discrete voltage vectors is depicted by small circles, with yellow circles referring to $\boldsymbol{v}(k) \in \boldsymbol{\mathcal{X}}_{\boldsymbol{v}}$ and blue ones to $\boldsymbol{v}(k) \notin \boldsymbol{\mathcal{X}}_{\boldsymbol{v}}$.

MPDCC chooses the voltage vector $\boldsymbol{v}(k)$ in an optimal manner. For that purpose, an objective function needs to be formulated and an optimization problem is to be solved, as shown in the next section.

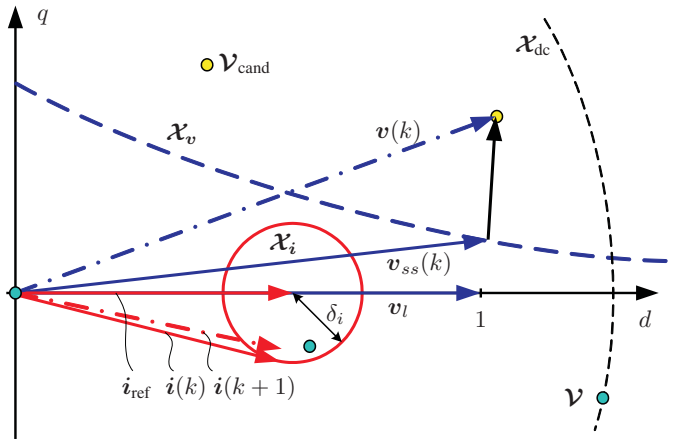

Fig. 2: Control principle of direct current control in the dq reference frame, when hitting the current bound

D. Optimization Problem

Writing the above control problem as a closed-form optimization problem leads to

$$J^*(\boldsymbol{x}(k), \boldsymbol{u}(k-1)) = \min_{\boldsymbol{U}(k)} \big(J_{\mathrm{sw}} + J_{\mathrm{bnd}}\big) \tag{12a}$$

$$\text{s.t. } \boldsymbol{x}(\ell+1) = \boldsymbol{A}\boldsymbol{x}(\ell) + \boldsymbol{B}\boldsymbol{u}(\ell) \tag{12b}$$

$$\boldsymbol{C}\boldsymbol{x}(\ell+1) \in \boldsymbol{\mathcal{X}}_i(\ell+1) \quad \text{or} \quad \boldsymbol{\epsilon}_i(\ell+1) < \boldsymbol{\epsilon}_i(\ell) \tag{12c}$$

$$\boldsymbol{u}(\ell) \in \boldsymbol{\mathcal{U}}\,, \tag{12d}$$

$$\forall \ell = k, \ldots, k + N_p - 1\,, \tag{12e}$$

with J^* denoting the minimum of the objective function $J = J_{\mathrm{sw}} + J_{\mathrm{bnd}}$. The sequence of control inputs $\boldsymbol{U}(k) = [\boldsymbol{u}^T(k), \boldsymbol{u}^T(k+1) \ldots, \boldsymbol{u}^T(k+N_p-1)]^T$ over the prediction horizon N_p represents the sequence of converter switch positions the controller decides upon. The objective function (12a) is minimized subject to the dynamical evolution of the load model (12b) and the constraints (12c) and (12d). The variables and matrices in (12) will be defined in the remainder of this section.

E. Objective Function

The objective function captures the switching effort, namely

$$J_{\mathrm{sw}} = \frac{1}{N_p T_s} \sum_{\ell=k}^{k+N_p-1} ||\Delta \boldsymbol{u}(\ell)||_1 \tag{13}$$

represents the sum of the switching transitions (number of commutations) over the prediction horizon N_p divided by the length of the horizon $N_p T_s$—it thus approximates the short-term switching frequency. Alternatively, the switching (power) losses can be represented, as shown for example in [9].

F. Internal Prediction Model

We opt to state the internal prediction model in stationary and orthogonal coordinates. The load current and voltage are chosen as the state vector $\boldsymbol{x} = [\boldsymbol{i}_{\alpha\beta}\ \boldsymbol{v}_{l,\alpha\beta}]^T$. The three-phase switch position constitutes the input vector $\boldsymbol{u} = \boldsymbol{u}_{abc}$, and $\boldsymbol{y} =$

$\boldsymbol{i}_{\alpha\beta}$ the output vector. Rewriting the continuous-time equations (4) and (5) in state-space form leads to

$$\frac{\mathrm{d}\boldsymbol{x}}{\mathrm{d}t}(t) = \boldsymbol{F}\boldsymbol{x}(t) + \boldsymbol{G}\boldsymbol{u}(t) \tag{14a}$$

$$\boldsymbol{y}(t) = \boldsymbol{C}\boldsymbol{x}(t)\,, \tag{14b}$$

with

$$\boldsymbol{F} = \begin{bmatrix} -\frac{R}{X_l}\boldsymbol{I} & -\frac{1}{X_l}\boldsymbol{I} \\ \boldsymbol{0} & \omega_e\boldsymbol{\Upsilon} \end{bmatrix}\,,\quad \boldsymbol{G} = \frac{V_{\mathrm{dc}}}{2X_l}\begin{bmatrix} \boldsymbol{P}(0) \\ \boldsymbol{0} \end{bmatrix}\,,\quad \boldsymbol{C} = \boldsymbol{I}\,. \tag{15}$$

Here, $\boldsymbol{I}$ denotes identity matrices and $\boldsymbol{0}$ zero matrices of appropriate dimensions. The exact Euler discretization method can be used to derive the discrete-time matrices $\boldsymbol{A} = \boldsymbol{e}^{\boldsymbol{F}T_s}$ and $\boldsymbol{B} = -\boldsymbol{F}^{-1}(\boldsymbol{I} - \boldsymbol{A})\boldsymbol{G}$ for the discrete-time state-space representation of the prediction model (12b), with $\boldsymbol{e}$ denoting the matrix exponential.

G. Constraints

If at time-step k the current falls within its bound $\boldsymbol{\mathcal{X}}_i$ as defined in (7), then it is required to remain within it. This is the standard case during steady-state operation. If, however, at time-step k the current violates its bound, then it has to move closer to the bound at every time-step ℓ within the prediction horizon, where $\ell = k, \ldots, k + N_p - 1$.

The constraint (12d) limits the control input $\boldsymbol{u}$ to the set of integers $\boldsymbol{\mathcal{U}}$. This constraint has to be met at every time-step ℓ within the prediction horizon.

IV. Model Predictive Direct Current Control

A. The MPDCC Solution Approach

The above optimization problem can be solved in real-time by a tailored approach, to which we refer as model predictive direct current control (MPDCC) [13]. MPDCC relies on the fact that switching is mainly required in the vicinity of the bound or when the bound has been violated. When the current is well within the bound, switching is not required and the switch position is frozen.

This gives rise to two different prediction horizons—the switching horizon (the number of switching instants within the horizon, i.e. the controller's degree of freedom) and the prediction horizon N_p (the number of time-steps MPDCC looks into the future). Between the switching instants the switch positions are frozen and the load behavior is extrapolated until the bound is hit. The concept of extrapolation leads to long prediction horizons (typically 100 time-steps), while the switching horizon is very short (usually one to three). The switching horizon is composed of the elements 'S' and 'E', which stand for 'switch' and 'extrapolate' (or more generally 'extend'), respectively. We use the task 'e' to add an optional extension leg to the switching horizon. For more details about the concept of the switching horizon, the reader is referred to [9].

B. MPDCC Algorithm

Given the pair $\boldsymbol{x}(k)$ and $\boldsymbol{u}(k-1)$, i.e. the load's state vector and the previously chosen converter switch position, the optimal control input $\boldsymbol{u}^*(k)$ can be computed according to the following procedure.

1) Initialize the root node with the current state vector $\boldsymbol{x}(k)$, the switch position $\boldsymbol{u}(k-1)$ and the switching horizon. Push the root node onto the stack.

2a) Take the top node with a non-empty switching horizon from the stack.

2b) Read out the first element. For 'S', branch on all feasible switching transitions, according to (12d). Use the internal prediction model (12b) to compute the state vector at the next time-step. For 'E', extend the trajectories either by using extrapolation, as detailed in [8], [16], or by using extrapolation with interpolation, as proposed in [27].

2c) Keep only the switching sequences that meet (12c).

2d) Push these sequences onto the stack.

2e) Stop if there are no more nodes with non-empty switching horizons. The result of this are the switching sequences $\boldsymbol{U}^i(k)$ over the variable-length prediction horizons N_p^i, where $i \in \mathcal{I}$ and $\mathcal{I}$ is an index set.

3) Compute for each sequence $i \in \mathcal{I}$ the associated cost J_i, as defined in (12a).

4) Choose the switching sequence $\boldsymbol{U}^* = \boldsymbol{U}^i(k)$ with the minimal cost, where $i = \arg\min_{i\in\mathcal{I}} J_i$.

5) Apply (only) the first switch position $\boldsymbol{u}^*(k)$ out of this sequence and execute the above procedure again at the next time-step $k+1$.

For an in-depth description and analysis of this algorithm, which is used with minor variations for the whole MPDxC family, the reader is referred to [9], [16] and [13]. It is straightforward to consider the balancing of a neutral point potential, see e.g. [9], [16], and of other internal voltages of the converter, as shown in [14]. Branch and bound techniques can be used to reduce the computation time by an order of magnitude [11].

V. Stability

From a mathematical point of view, the states of the system model (10)–(11) will in general be contained in a bounded (though large) set and, thus, be *practically stable*. However, when applying closed-loop control to a real converter, the load currents may exceed the safe operating range. To avoid this crucial issue, in the sequel we will provide a method that not only ensures practical stability, but also allows one to keep the currents within a safe region. Our analysis follows in a fairly direct manner from the way the MPDCC algorithm has been designed.

A. Convergence to the Bound

We start by showing that, when the current violates the bound, the current error is reduced at each time step and the current is brought closer to the bound (this is known as practical stability or ultimate boundedness [18]). This is directly imposed by the MPDCC algorithm, specifically by

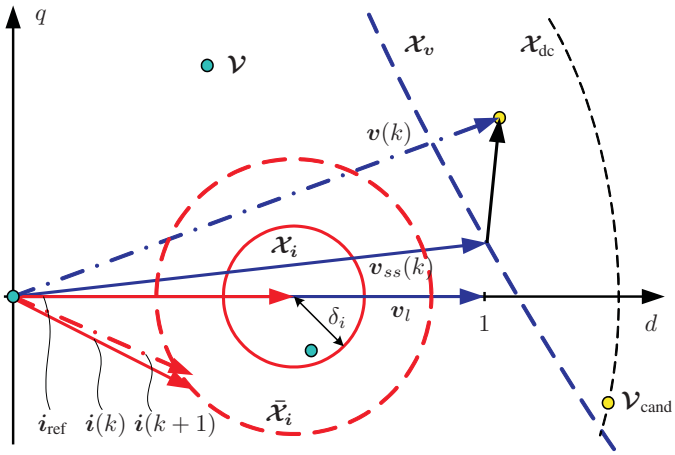

Fig. 3: Control principle of direct current control in the dq reference frame, when violating the current bound

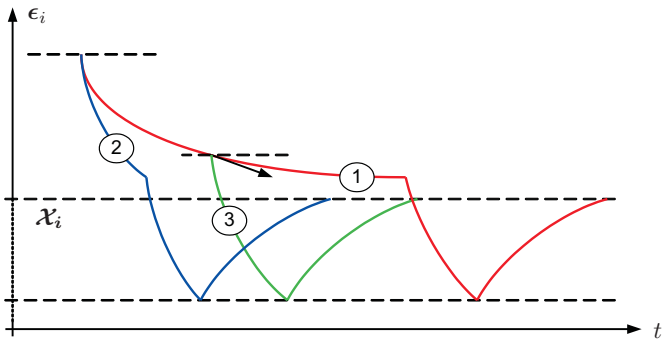

Fig. 4: Closed-loop current trajectories versus the time-axis t for three different scenarios: 1) standard MPDCC with $J_{\text{bnd}} = 0$; 2) MPDCC with $J_{\text{bnd}} > 0$ to increase the convergence rate to the set $\boldsymbol{\mathcal{X}}_i$; 3) robust MPDCC with $J_{\text{bnd}} = 0$

the second constraint in (12c). Only voltage vectors are considered, which fulfill this condition. We refer to such voltage vectors as candidates. Voltage vectors that are predicted to maintain or even increase the degree of the violation, are not further considered and are not part of the set $\mathcal{I}$.

The set of candidate voltage vectors is given by $\boldsymbol{\mathcal{V}}_{\text{cand}} = \boldsymbol{\mathcal{X}}_v \cap \boldsymbol{\mathcal{V}}$, as defined in Sect. III. Since the load voltage $\boldsymbol{v}_l$ is at most of magnitude one and because the resistive-inductive voltage drop over the load impedance is limited, $\boldsymbol{v}_{ss}$ is close to $\boldsymbol{v}_l$ and thus always almost one. By definition, $\boldsymbol{v}_{ss}$ is included in the enclosure of $\boldsymbol{\mathcal{X}}_v$. In addition, for small sampling intervals T_s, the circular set $\boldsymbol{\mathcal{X}}_v$ approaches a halfspace. Since the converter under consideration utilizes symmetrical voltage steps, the discrete voltage vectors are uniformly distributed in $\boldsymbol{\mathcal{X}}_{\text{dc}}$. For sufficiently high dc-link voltages, say 1.8 pu and more, the set $\boldsymbol{\mathcal{V}}_{\text{cand}}$ is always non-empty. As a result, there always exists at least one voltage vector $\boldsymbol{v}(k) \in \boldsymbol{\mathcal{V}}_{\text{cand}} \neq \emptyset$ that moves the current closer to its bound, i.e.

$$||\boldsymbol{i}(k+1) - \boldsymbol{i}_{\text{ref}}||_2 < ||\boldsymbol{i}(k) - \boldsymbol{i}_{\text{ref}}||_2 \,. \tag{16}$$

The set of currents at time-step $k+1$, for which (16) holds, is the circular set

$$\boldsymbol{i} \in \bar{\boldsymbol{\mathcal{X}}}_i \,, \quad \bar{\boldsymbol{\mathcal{X}}}_i = \{\boldsymbol{i} \in \mathbb{R}^2 : ||\boldsymbol{i}_{\text{ref}} - \boldsymbol{i}||_2 \leq \bar{\delta}_i\} \tag{17}$$

with $\bar{\delta}_i = ||\boldsymbol{i}_{\text{ref}} - \boldsymbol{i}(k)||_2$. The set's enclosure is shown as a dashed (red) circle in Fig. 3.

In order to increase the convergence rate an additional term may be added to the objective function, such as [12]

$$J_{\text{bnd}} = \begin{cases} 0 & \text{if } \boldsymbol{i} \in \boldsymbol{\mathcal{X}}_i \\ \gamma \epsilon_i^2 & \text{else} \,. \end{cases} \tag{18}$$

This expression can be interpreted as a piecewise quadratic Lyapunov function, which quadratically penalizes the degree of the bound violation and is zero when the current is within its bound. As was shown in [12], this term enforces a faster convergence rate.

B. Staying within the Bound

Once the current has entered its bound, i.e. $\boldsymbol{i} \in \boldsymbol{\mathcal{X}}_i$, the constraint $\boldsymbol{C}\boldsymbol{x}(\ell+1) \in \boldsymbol{\mathcal{X}}_i(\ell+1)$ is imposed on the predicted current trajectory, see (12c) in the MPDCC optimization problem. Only voltage vectors $\boldsymbol{v}(k) \in \boldsymbol{\mathcal{X}}_v$ are considered which meet this condition. Using the same arguments as in the previous section, one can show that $\boldsymbol{\mathcal{X}}_{\text{cand}}$ is non-empty. We conclude that there always exists at least one voltage vector $\boldsymbol{v}(k) \in \boldsymbol{\mathcal{V}}_{\text{cand}} \neq \emptyset$ that keeps the current within its bound, i.e.

$$\boldsymbol{i}(k) \in \boldsymbol{\mathcal{X}}_i \Rightarrow \boldsymbol{i}(k+1) \in \boldsymbol{\mathcal{X}}_i$$

The set $\boldsymbol{\mathcal{X}}_i$ is thus a control invariant set [5].

VI. Robust Stability

In the sequel, we will show how the original algorithm can be modified to account for model imperfections. For that purpose, we will assume that the prediction model is affected by additive parameter uncertainties of the form

$$\boldsymbol{x}_{\text{unc}}(k+1) = (\boldsymbol{A} + \tilde{\boldsymbol{A}})\boldsymbol{x}(k) + (\boldsymbol{B} + \tilde{\boldsymbol{B}})\boldsymbol{u}(k) \,, \tag{19}$$

where the matrices $\boldsymbol{A}$ and $\boldsymbol{B}$ represent the nominal model, and $\tilde{\boldsymbol{A}}$ and $\tilde{\boldsymbol{B}}$ capture parameter uncertainties of the model.

Substituting (19) into $||\boldsymbol{x}_{\text{unc}}(k+1) - \boldsymbol{x}_{\text{ref}}||_2$ leads to

$$\begin{aligned} ||\boldsymbol{x}_{\text{unc}}(k+1) - \boldsymbol{x}_{\text{ref}}||_2 \leq\, & ||\boldsymbol{x}_{\text{nom}}(k+1) - \boldsymbol{x}_{\text{ref}}||_2 \\ & + ||\tilde{\boldsymbol{A}}\boldsymbol{x}(k) + \tilde{\boldsymbol{B}}\boldsymbol{u}(k)||_2 \,, \end{aligned} \tag{20}$$

where we have introduced $\boldsymbol{x}_{\text{nom}}(k+1) = \boldsymbol{A}\boldsymbol{x}(k) + \boldsymbol{B}\boldsymbol{u}(k)$. The deviation from the reference at $k+1$ is thus bounded by the sum of two terms—the nominal response and an uncertainty term, which is a function of the state vector and the input. On the uncertainty term we introduce the upper bound

$$||\tilde{\boldsymbol{A}}\boldsymbol{x}(k) + \tilde{\boldsymbol{B}}\boldsymbol{u}(k)||_2 \leq p_1 ||\boldsymbol{x}(k)||_2 + p_2 \,. \tag{21}$$

To ensure (robust) convergence to the bound in the presence of additive parameter uncertainties, the right hand side of (20) has to be strictly less than $||\boldsymbol{x}(k) - \boldsymbol{x}_{\text{ref}}||_2$, i.e.

$$||\boldsymbol{x}_{\text{nom}}(k+1) - \boldsymbol{x}_{\text{ref}}||_2 + p_1 ||\boldsymbol{x}(k)||_2 + p_2 < ||\boldsymbol{x}(k) - \boldsymbol{x}_{\text{ref}}||_2 \,. \tag{22}$$

This is equivalent to

$$\epsilon_i(k+1) + p_1 ||\boldsymbol{x}(k)||_2 + p_2 < \epsilon_i(k) \tag{23}$$

To ensure robust stability, when the current is outside of the bound, the constraint on the right hand side in (12c) is to be replaced by (23). This ensures that only voltage vectors are selected that point with a certain minimum angle towards the current reference, i.e. the center of the circular bound. To ensure robust stability, it suffices to impose (23) only on the first step in the prediction interval from k to $k+1$.

Accordingly, when the current is within its bound, the constraint on the left hand side in (12c) needs to be modified. Specifically, the constraint at $k+1$ is replaced by $\boldsymbol{x}(k+1) \in \tilde{\boldsymbol{\mathcal{X}}}_i$, where $\tilde{\boldsymbol{\mathcal{X}}}_i$ uses the radius

$$\tilde{\delta}_i = \delta_i - p_1 ||\boldsymbol{x}(k)||_2 - p_2 \,. \tag{24}$$

As a result, $\tilde{\boldsymbol{\mathcal{X}}}_i$ is a subset of $\boldsymbol{\mathcal{X}}_i$. This ensures robust stability once we are within the bounds.

The robustification of MPDCC is visualized in Fig. 4, which shows three abstract current trajectories versus time for three different scenarios, with the current initially violating its dashed (black) bound. Using standard MPDCC with $J_{\text{bnd}} = 0$ might lead to slow convergence to the bound. Adding J_{bnd} to the objective function with $\gamma > 0$ enforces switching when the current is out of its bound and the convergence rate drops. When using robust MPDCC, a minimum convergence rate is to be maintained, so as to ensure convergence to the bound despite parameter uncertainties, see Fig. 4.

To deal with bounded input and measurement noise, similar techniques can be adopted to establish convergence of converter states, cf., [24].

VII. Conclusions

This work has shown that MPDCC readily ensures closed-loop stability by the way the control algorithm has been formulated. In particular, we have established that—through minor modifications—robust stability in the presence of bounded uncertainties in converter parameters can be guaranteed.

The stability argument in this paper can be directly extended to hexagon-shaped bounds and to the other members of the MPDxC family, notably to MPDTC, MPDPC and MPDBC. MPDTC, for example, imposes upper and lower bounds on the electromagnetic torque and the stator flux magnitude, respectively. Since these bounds can be translated into equivalent stator currents, a control problem *equivalent* to MPDTC can be formulated by imposing bounds on the stator currents, as shown in [13]. These bounds have, however, a non-trivial shape. Similar arguments can be made for MPDPC and MPDBC. Moreover, instead of an active RL load, an induction machine can be considered, with the stability investigation focusing on the machine's stator currents. Similar arguments can be made for synchronous machines.

References

[1] R. P. Aguilera and D. E. Quevedo. On stability and performance of finite control set MPC for power converters. In *Workshop on Pred. Control of Electr. Drives and Power Electron.*, pages 55–62, Munich, Germany, Oct. 2011.

[2] R. P. Aguilera and D. E. Quevedo. On the stability of MPC with a finite input alphabet. In *IFAC Symp.*, pages 7975–7980, Milano, Italy, Aug. 2011.

[3] R. P. Aguilera, D. E. Quevedo, T. J. Summers, and P. Lezana. Predictive control algorithm robustness for achieving fault tolerance in multicell converters. In *Proc. IEEE Ind. Electron.*, pages 3302–3308, Orlando, FL, Nov. 2008.

[4] A. Bemporad, M. Morari, V. Dua, and E. N. Pistikopoulos. The explicit linear quadratic regulator for constrained systems. *Automatica*, 38(1):3–20, Jan. 2002.

[5] F. Blanchini and S. Miani. *Set-Theoretic Methods in Control*. Systems & control. Birkhäuser Boston, 2007.

[6] G. S. Buja. Optimum output waveforms in PWM inverters. *IEEE Trans. Ind. Appl.*, 16(6):830–836, Nov./Dec. 1980.

[7] P. Cortés, M. P. Kazmierkowski, R. M. Kennel, D. E. Quevedo, and J. Rodríguez. Predictive control in power electronics and drives. *IEEE Trans. Ind. Electron.*, 55(12):4312–4324, Dec. 2008.

[8] T. Geyer. *Low Complexity Model Predictive Control in Power Electronics and Power Systems*. PhD thesis, Autom. Control Lab. ETH Zurich, 2005.

[9] T. Geyer. Generalized model predictive direct torque control: Long prediction horizons and minimization of switching losses. In *Proc. IEEE Conf. Decis. Control*, pages 6799–6804, Shanghai, China, Dec. 2009.

[10] T. Geyer. A comparison of control and modulation schemes for medium-voltage drives: emerging predictive control concepts versus PWM-based schemes. *IEEE Trans. Ind. Appl.*, 47(3):1380–1389, May/Jun. 2011.

[11] T. Geyer. Computationally efficient model predictive direct torque control. *IEEE Trans. Power Electron.*, 26(10):2804–2816, Oct. 2011.

[12] T. Geyer. Model predictive direct torque control: Derivation and analysis of the explicit control law. In *Proc. IEEE Energy Convers. Congr. Expo.*, pages 355–362, Phoenix, AZ, USA, Sep. 2011.

[13] T. Geyer. Model predictive direct current control: formulation of the stator current bounds and the concept of the switching horizon. *IEEE Ind. Appl. Mag.*, 18(2):47–59, Mar./Apr. 2012.

[14] T. Geyer and S. Mastellone. Model predictive direct torque control of a five-level ANPC converter drive system. In *Proc. IEEE Energy Convers. Congr. Expo.*, pages 363–370, Phoenix, AZ, USA, Sep. 2011.

[15] T. Geyer, G. Papafotiou, and M. Morari. Hybrid model predictive control of the step-down dc-dc converter. *IEEE Trans. Contr. Syst. Technol.*, 16(6):1112–1124, Nov. 2008.

[16] T. Geyer, G. Papafotiou, and M. Morari. Model predictive direct torque control—Part I: Concept, algorithm and analysis. *IEEE Trans. Ind. Electron.*, 56(6):1894–1905, Jun. 2009.

[17] T. Geyer, J. Scoltock, and U. Madawala. Model predictive direct power control for grid-connected converters. In *Proc. IEEE Ind. Electron.*, Melbourne, Australia, Nov. 2011.

[18] H. Khalil. *Nonlinear Systems*. Prentice-Hall, 3rd edition edition, 2001.

[19] F. Kieferndorf, P. Karamanakos, Ph. Bader, N. Oikonomou, and T. Geyer. Model predictive control of the internal voltages of a five-level active neutral point clamped converter. In *Proc. IEEE Energy Convers. Congr. Expo.*, Raleigh, NC, USA, Sep. 2012.

[20] M. Lazar and W. P. M. H. Heemels. Predictive control of hybrid systems: Input-to-state stability results for sub-optimal solutions. *Automatica*, 45(1):180–185, Jan. 2009.

[21] P. Lezana, R. P. Aguilera, and D. E. Quevedo. Model predictive control of an asymmetric flying capacitor converter. *IEEE Trans. Ind. Electron.*, 56(6):1839–1846, Jun. 2009.

[22] D. E. Quevedo, R. P. Aguilera, M. A. Pérez, P. Cortés, and R. Lizana. Model predictive control of an AFE rectifier with dynamic references. *IEEE Trans. Power Electron.*, 27(7):3128–3136, Jul. 2012.

[23] D. E. Quevedo, G. C. Goodwin, and J. A. De Doná. Finite constraint set receding horizon quadratic control. *Int. J. of Robust Nonlinear Control*, 14(4):355–377, Mar. 2004.

[24] B. J. P. Roset, W. P. M. H. Heemels, M. Lazar, and H. Nijmeijer. On robustness of constrained discrete-time systems to state measurement errors. *Automatica*, 44:1161–1165, 2008.

[25] M. Senesky, G. Eirea, and T. J. Koo. Hybrid modelling and control of power electronics. In A. Pnueli and O. Maler, editors, *Hybrid Syst.: Comput. and Control*, volume 2623 of *LNCS*, pages 450–465. Springer, 2003.

[26] I. Takahashi and T. Noguchi. A new quick response and high efficiency control strategy for the induction motor. *IEEE Trans. Ind. Appl.*, 22(2):820–827, Sep./Oct. 1986.

[27] Y. Zeinaly, T. Geyer, and B. Egardt. Trajectory extension methods for model predictive direct torque control. In *Proc. App. Power Electron. Conf. and Expo.*, pages 1667–1674, Fort Worth, TX, USA, Mar. 2011.